NANOSYSTEMS: PHYSICS, CHEMISTRY, MATHEMATICS, 2020, 11 (4), P. 424–433

MoO_3:In_2O_3 binary oxide thin films as CO gas sensor

Nimba Kothawade[1], Jitendra Borse[2], Vikas Deshmane[3], Arun Patil[4]

[1]Department of Physics, Arts, Commerce and Science College, Kalwan (Manur), Nashik, India

[2]Department of Physics, Late Pushpadevi Patil Arts and Science College,Risod. India

[3]Department of Physics, SICES Degree College, Ambernath, Thane, Maharashtra, India

[4]Research centre in electronics science, LVH College, Panchavati, Nashik, India

jaborse@gmail.com

DOI 10.17586/2220-8054-2020-11-4-424-433

Thin films of binary oxides (MoO_3–In_2O_3) of different normality proportions of 0.1N:0.1N, 0.2N:0.1N, 0.3N:0.1N, 0.1N:0.2N, 0.2N:0.2N, 0.3N:0.2N, 0.1N:0.3N, 0.2N:0.3N and 0.3N:0.3N were prepared by a spray pyrolysis technique on glass substrates at 400°C. The prepared films were characterized using X-ray diffraction (XRD), scanning electron microscope (SEM) and energy dispersive analysis by x-ray spectra (EDAX). The electrical and gas sensing properties of the films were studied using static gas sensing apparatus. The electrical analysis confirmed that the resistivity of films increased by adding MoO_3 as the dopant in In_2O_3. The maximum resistivity of film was found 1.75×10^4 Ωm for 0.3N (MoO_3) and 0.1N (In_2O_3) binary oxide films. The films were tested against five different target gases. The composition ratio 0.3N:0.1N films showed the 70.50% sensitivity for 300 ppm CO gas at 150°C. The response time (15 s) and recovery time (25 s) was found to be quick. The % selectivity was maximum for 0.3N:0.1N films.

Keywords: MoO_3, In_2O_3, spray pyrolysis, carbon monoxide, gas sensor.

Received: 18 March 2020

Revised: 17 August 2020

1. Introduction

Indium oxide (In_2O_3) and molybdenum trioxide (MoO_3) are common metal oxides used in gas sensing. Recent research has indicated that In_2O_3 and MoO_3 films have excellent responses to oxidizing gases [1–8]. In_2O_3 based sensors can detect reducing gases, such as methane (CH_4) and carbon monoxide (CO) [9–12]. It was found that In_2O_3 based sensors may have excellent selectivity to CO in the presence of hydrogen (H_2) in the surrounding atmosphere. According to Yamaura et al., In_2O_3 and cobalt oxide heterojunction performed like CO gas sensor [11, 12]. Recently, the use of mixed binary metal oxides for gas sensing application has increased. The binary mixtures of In_2O_3 and MoO_3 may lead to improved gas sensing properties.

Increased industrialization has caused an increase in pollution. Carbon monoxide is one of the prominent pollutant gas. It is very important to design CO selective sensors. The undoped MoO_3 exhibits fast response for nitrogen dioxide (NO_2) and excellent sensitivity to CO in the temperatures range from 200 – 400°C as reported by Ferroni et al. [13, 14]. The metal oxide semiconductor (MOS) such as In_2O_3, has been reported to have high sensitivities to many gases such as hydrogen (H_2), carbon monoxide (CO), nitrogen dioxide (NO_2), ammonia (NH_3), ozone (O_3), and chlorine (Cl_2) [15–18].

X. Liu et al. (2018) reported indium oxide and molybdenum disulfide nanocomposite for ethanol sensing [19]. H. Li et al. also carried out acetone vapor sensing study of molybdenum disulfide and tungsten oxide. The operating temperature was about 100°C [20].

Cobalt oxide and molybdenum disulfide was also reported as methane sensor at 170°C by D. Zhang et. al. [21]. The gas sensing study of indium oxide and molybdenum disulfide has been reported by many studies but the metal oxide nanocomposite of indium oxide and molybdenum oxide has been rarely reported as gas sensing materials. In the current study authors tried to study gas sensing performance of molybdenum oxide doped indium oxide thin films. The current study employed a spray pyrolysis method for the preparation of MoO_3 added In_2O_3 thin films. The present investigation reports MoO_3-In_2O_3 binary oxide thin films with good sensitivity to CO gas.

2. Experimental

Thin films of MoO_3–In_2O_3 were prepared by using a spray pyrolysis technique. All chemicals of analytical reagent (AR) grade were used. For the preparation of 0.1N, 0.2N, 0.3N In_2O_3 precursor, 0.278, 0.556, 0.834 gm of $InCl_3$ respectively was dissolved in 10 ml of ethanol and stirred vigorously for 10 minutes using magnetic stirrer. For the preparation of 0.1N, 0.2N, 0.3N MoO_3 solutions, 0.274, 0.548 and 0.822 gm of $MoCl_5$ was dissolved in 10 ml of ethanol and stirred vigorously using magnetic stirrer. These precursors were mixed with MoO_3:In_2O_3 normality ratios of 0.1:0.1, 0.2:0.1, 0.3:0.1, 0.1:0.2, 0.2:0.2, 0.3:0.2, 0.1:0.3, 0.2:0.3, and 0.3:0.3. These samples were referred as 0.1:0.1, 0.2:0.1, 0.3:0.1, 0.1:0.2, 0.2:0.2, 0.3:0.2, 0.1:0.3, 0.2:0.3, and 0.3:0.3 respectively during subsequent communication. Then mixed precursors were stirred for 30 minutes at 40°C. These mixed precursors were then used for spray pyrolysis. Films were prepared on a glass substrate at 400°C. The solution was sprayed on a glass substrate with a spray interval of 10 seconds. Thus prepared films were characterized using X-ray diffraction (XRD) (D8 Advance, Bruker-AXS), scanning electron microscopy (SEM) (JEOL JSM-6360A) and energy dispersive analysis of X-ray (EDAX) at S. P. Pune University. The electrical and gas sensing parameters were analyzed using static gas sensing apparatus. The average crystallite size (D) was determined from XRD pattern using following Debye Scherer equation [22]:

$$D = \frac{0.9\lambda}{\beta \cos\theta}(\Omega m). \tag{1}$$

Where β is full angular width at half maximum and λ is the wavelength of X-rays [23].

The DC resistance of the films was measured using the half-bridge method under aerobic conditions at different temperatures. The resistivity (ρ) of the deposited films with a thickness (t), breadth (b), length (l) was determined by using the following equation:

$$\rho = \frac{Rbt}{l}\ (\Omega\mathrm{m}). \tag{2}$$

Here, R is the resistance. The temperature coefficient of resistance a_{TCR} was determined by using the formula:

$$a_{TCR} = \frac{1}{R_0}\frac{\Delta R}{\Delta T}(^oK^{-1}). \tag{3}$$

Here, ΔR was the change in resistance between temperature and ΔT was a corresponding change in temperature and R_0 was the resistance of the film at room temperature [24].

The activation energy of film samples was determined from the Arrhenius equation:

$$\mathrm{R} = R_0 \exp\frac{-\Delta E}{kT}, \tag{4}$$

where ΔE was the activation energy of the electron transport in the conduction band (eV), K was the Boltzmann constant and T was absolute temperature.

The gas sensing studies were carried out in a static gas sensing system under normal laboratory conditions. The electrical resistance of films in the air (R_a) and in the presence of gas (R_g) was measured to evaluate the gas sensitivity (S) given by the formula.

$$S = \frac{|R_a - R_g|}{R_g}100. \tag{5}$$

The selectivity of the films for the particular gas with respect to other (γ) was determined by the relation [25]:

$$\gamma = \frac{S_{other\ gas}}{S_{target\ gas}} \cdot\ 100. \tag{6}$$

3. Result and discussions

3.1. X-ray diffraction analysis

MoO_3–In_2O_3 binary thin film were characterized using XRD. The Copper (Cu-Kα) source with wavelength of 1.54056 Å was used for the purpose. The XRD patterns of as-deposited 0.1:0.1, 0.2:0.1, 0.3:0.1, 0.1:0.2, 0.2:0.2, 0.3:0.2, 0.1:0.3, 0.2:0.3, and 0.3:0.3 MoO_3–In_2O_3 binary oxide films is shown in Fig. 1.

The major peaks were located at 2 theta values 26.68, 30.83, 33.04, 35.61, 51.27 and 60.83. According to JCPDS no. 42-0313, these peaks were of Indium Molybdenum Oxide. These peaks were along [220], [310], [320], [210], [331] and [521] planes according to JCPDS data. The [310] was the most preferred plane for the films. This was the preferential direction for crystal growth. The grain sizes were calculated using the Scherer formula. It was found that the grain size was in the 2 – 10 nm range. As the proportions of Molybdenum increased, certain peaks became prominent. This confirmed that with the addition of Molybdenum the crystallinity of the sample increased.

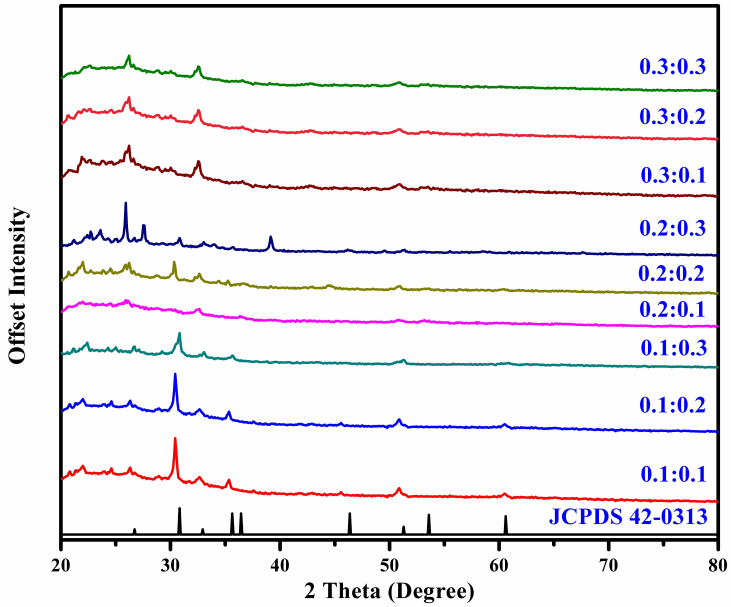

FIG. 1. XRD stack of 0.1:0.1, 0.1:0.2, 0.1:0.3, 0.2:0.1, 0.2:0.2, 0.2:0.3, 0.3:0.1, 0.3:0.2, and 0.3:0.3 MoO_3–In_2O_3 binary oxide films

3.2. Scanning electron microscopy

Figure 2(a–i) shows the SEM micrographs of 0.1:0.1, 0.2:0.1, 0.3:0.1, 0.1:0.2, 0.2:0.2, 0.3:0.2, 0.1:0.3, 0.2:0.3, and 0.3:0.3 MoO_3–In_2O_3 binary oxide films with 6K magnification. The 0.1:1, 0.2:0.2 and 0.3:0.3 films showed non-porous structure, whereas 0.1:0.3 and 0.3:0.1 showed porous structure. The intermediate cracks were also formed on the surface of the films. This porous nature and intermediate cracks facilitate adsorption of atmospheric oxygen as well the target gas molecules.

The particle size was calculated from SEM images using Image-J software. As a result, the average particles size of deposited films was changed with the variation of elemental composition. It is clear that the films have a uniform crystalline structure with average particle size in the range of 2550 – 255 nm, whereas the average particle size decreases by increasing the concentration of Mo doping content [26]. The decrease in average particle size improves surface to volume ratio. Higher is the surface to volume ratio, greater will be the adsorption probability.

3.3. Energy dispersive analysis of X-ray spectra

Figure 3(a–i) shows the energy dispersive analysis by X-ray spectra (EDAX) of MoO_3:In_2O_3 binary oxide thin film with different concentrations. The peaks corresponding to Molybdenum and Indium were observed in the spectra. This confirmed that molybdenum trioxide and indium oxide were present in the films. Minor peaks might be attributed to the impurities present or the substrate elements.

Table 1 demonstrates the elemental distribution observed in 0.1:0.1, 0.2:0.1, 0.3:0.1, 0.1:0.2, 0.2:0.2, 0.3:0.2, 0.1:0.3, 0.2:0.3, and 0.3:0.3 MoO_3–In_2O_3 binary films. It was evident that Indium and Molybdenum were present in thin films. The atomic percentage of elements such as oxygen (O), Molybdenum (Mo) and Indium (In) conveyed that the films were non-stoichiometric in nature. All of the prepared films were found to have excess oxygen. This excess oxygen might have been adsorbed from the atmosphere during the preparation of thin films at 400°C.

3.4. Electrical properties of MoO_3: In_2O_3 thin film

The effect of doping of MoO_3 into In_2O_3 in various normality ratios can affect the electrical properties pristine materials. Hence, the electrical properties of thin films of MoO_3:In_2O_3 binary oxides were studied using simple potential divider arrangement. The electrical properties like resistivity, temperature coefficient of resistance (TCR) and activation energy have been summarized in Table 2. A known resistance and sample to be tested were connected in series. The temperature of the surrounding of the thin film sample was varied in steps of 50°C and corresponding resistance was noted. The outcomes of the electrical study have been demonstrated in Fig. 4(a,b). Fig. 4(a) is a resistance versus temperature graph for 0.1:0.1, 0.2:0.1, 0.3:0.1, 0.1:0.2, 0.2:0.2, 0.3:0.2, 0.1:0.3, 0.2:0.3, and 0.3:0.3 MoO_3–In_2O_3 binary thin films.

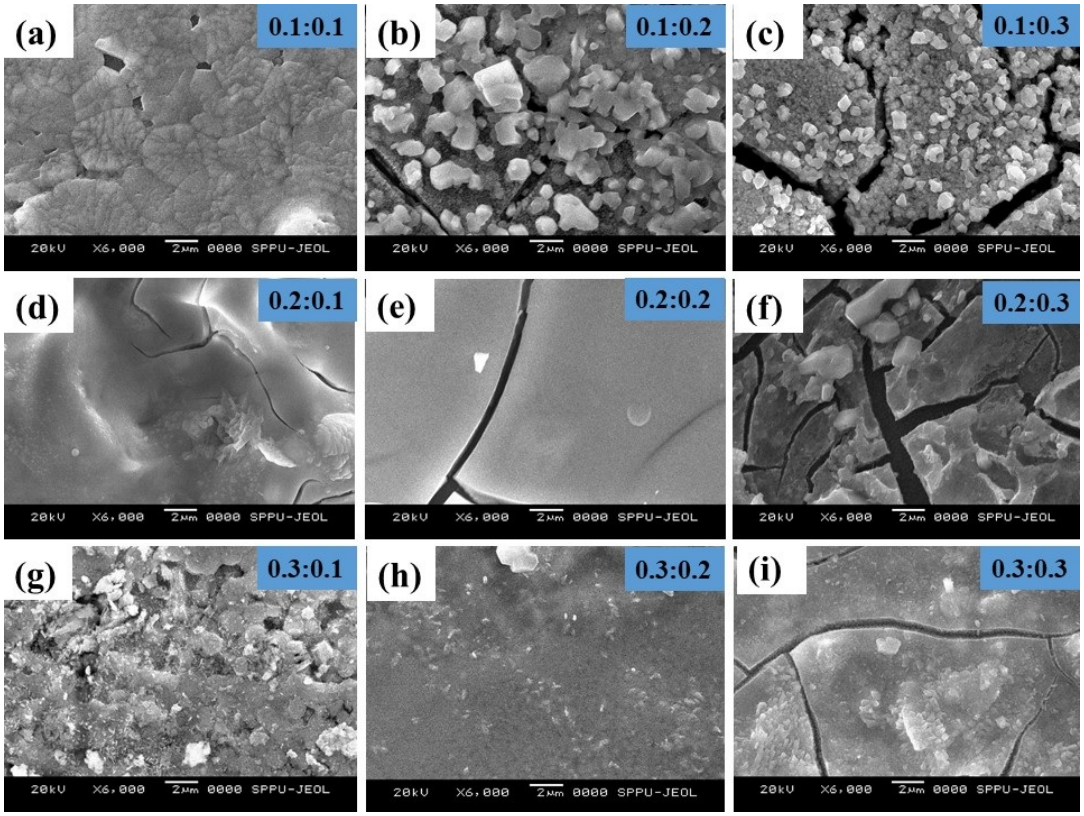

FIG. 2. SEM micrograph of (a) 0.1:0.1, (b) 0.1:0.2, (c) 0.1:0.3, (d) 0.2:0.1, (e) 0.2:0.2, (f) 0.2:0.3, (g) 0.3:0.1, (h) 0.3:0.2, and (i) 0.3:0.3 MoO_3–In_2O_3 binary oxide films

TABLE 1. The elemental distribution of 0.1:0.1, 0.2:0.1, 0.3:0.1, 0.1:0.2, 0.2:0.2, 0.3:0.2, 0.1:0.3, 0.2:0.3, and 0.3:0.3 MoO_3–In_2O_3 binary oxide films

		0.1N In_2O_3		0.2N In_2O_3		0.3N In_2O_3	
		Wt. %	Atomic %	Wt. %	Atomic %	Wt. %	Atomic %
0.1N	Oxygen	57.98	85.19	64.55	95.29	76.42	85.96
MoO_3	Mo	48.50	11.88	11.45	2.82	37.65	7.06
	In	14.29	2.92	9.18	1.89	44.50	6.97
0.2N	Oxygen	59.61	85.48	47.45	88.08	61.82	85.54
MoO_3	Mo	47.83	11.44	23.18	7.17	45.62	10.53
	In	15.44	3.08	18.34	4.74	20.43	3.94
0.3N	Oxygen	55.17	84.76	71.72	90.34	65.48	89.19
MoO_3	Mo	50.55	12.95	30.72	6.45	28.03	6.37
	In	10.69	2.29	18.28	3.21	23.41	4.44

As seen in Fig. 4a, the resistance of the films decreased with increase in temperature. The rate of decrease of resistance was high in the low-temperature region. At high temperatures, the film resistance nearly saturated to its lowest values. The films were having a negative temperature coefficient of resistance (equation 3). TCR for 0.1N:0.1N film was found $-0.01831/^\circ$K. The n-type semiconducting behavior of the pristine metal oxides MoO_3 and In_2O_3 were restored after mixing and annealing.

The resistivity measurements were carried out using equation 2. The resistivity was found to be increasing with the increase in MoO_3 content. The 0.3N MoO_3 and 0.1N In_2O_3 films exhibited maximum resistivity of $17.50\times10^3\Omega$. The resistivity of the film of compositional ratio 0.1N:0.1N was found to be $13.125\times10^3\Omega$m. The film showed $14.98\times10^3\Omega$m resistivity by adding 0.2N MoO_3 in 0.1N In_2O_3 and TCR was found to be $-0.01790/^\circ$K. However, the resistivity of film was found $17.50\times10^3\Omega$m by adding 0.3N MoO_3 in 0.1N In_2O_3 and TCR was $-0.02088/^\circ$K. As a

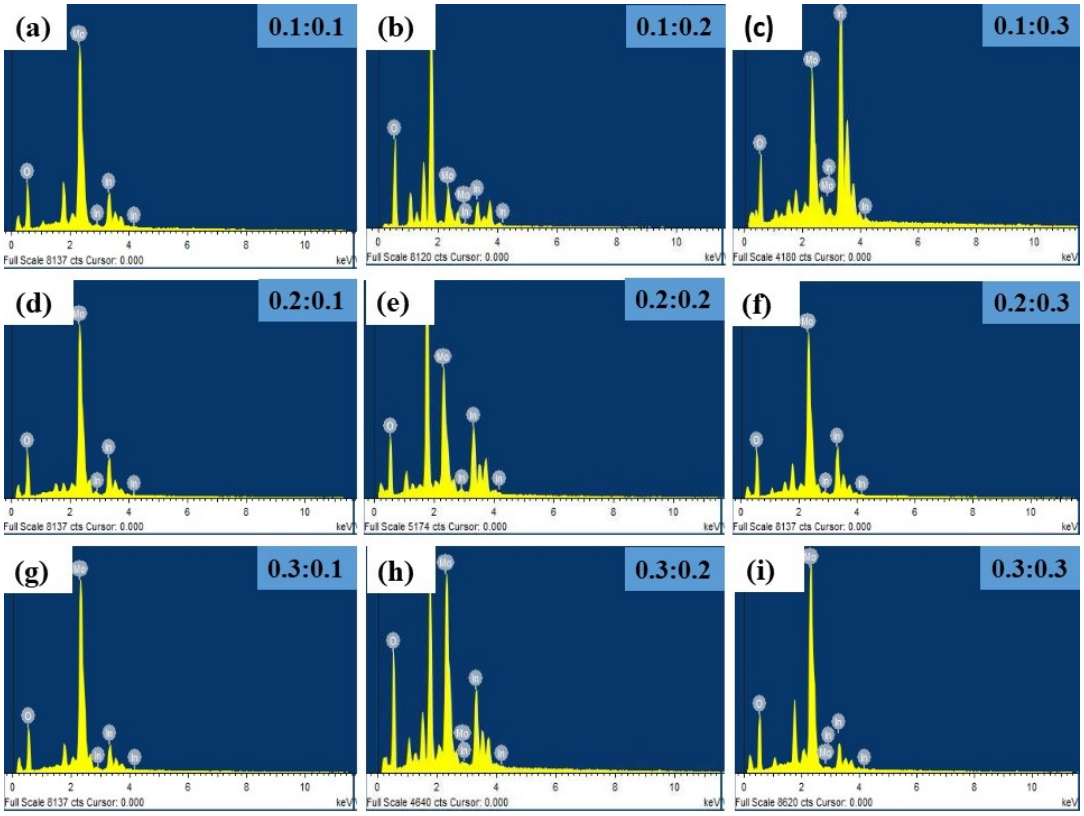

FIG. 3. EDS of (a) 0.1:0.1, (b) 0.1:0.2, (c) 0.1:0.3, (d) 0.2:0.1, (e) 0.2:0.2, (f) 0.2:0.3, (g) 0.3:0.1, (h) 0.3:0.2, and (i) 0.3:0.3 MoO_3–In_2O_3 binary oxide films

TABLE 2. Resistivity, TCR and activation energies in low and high temperature region for 0.1:0.1, 0.2:0.1, 0.3:0.1, 0.1:0.2, 0.2:0.2, 0.3:0.2, 0.1:0.3, 0.2:0.3, and 0.3:0.3 MoO_3–In_2O_3 binary oxide films

Mo:In Normality Ratio	Resistivity (X 10^4 Ω.m)	TCR (per deg. Kelvin)	Activation Energy (eV)	
			Low Temp. Region	High Temp. Region
0.1 : 0.1	13.13	–0.018	0.0162	0.6761
0.2 : 0.1	14.98	–0.018	0.0171	0.5773
0.3 : 0.1	17.50	–0.012	0.0143	0.4172
0.1 : 0.2	10.50	–0.030	0.0299	0.7424
0.2 : 0.2	11.66	–0.020	0.0366	0.6362
0.3 : 0.2	12.36	–0.015	0.0284	0.4911
0.1 : 0.3	12.33	–0.018	0.0220	0.7983
0.2 : 0.3	16.14	–0.016	0.0108	0.6553
0.3 : 0.3	17.50	–0.011	0.0283	0.4695

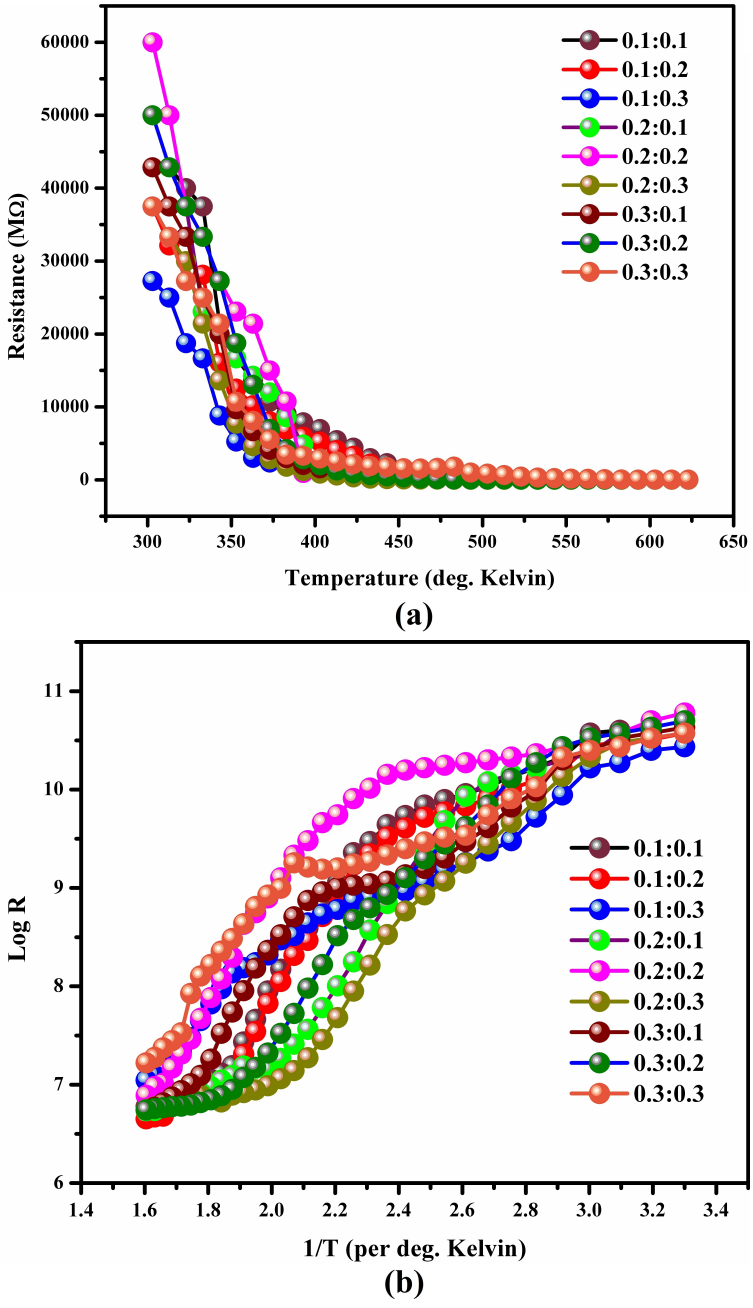

FIG. 4. (a) Resistance versus temperature for 0.1:0.1, 0.2:0.1, 0.3:0.1, 0.1:0.2, 0.2:0.2, 0.3:0.2, 0.1:0.3, 0.2:0.3, and 0.3:0.3 MoO_3–In_2O_3 binary oxide films. (b) Logarithm of resistance versus 1/Temperature graph for 0.1:0.1, 0.2:0.1, 0.3:0.1, 0.1:0.2, 0.2:0.2, 0.3:0.2, 0.1:0.3, 0.2:0.3, and 0.3:0.3 MoO_3–In_2O_3 binary oxide films

result, the film exhibited the highest resistivity and TCR by adding 0.3N MoO_3 in 0.1N In_2O_3. When the concentration of In_2O_3 was constant, the addition of different concentration of MoO_3 (0.1N–0.3N) affected resistivity and TCR of films.

Fig. 4(b) showed the plot of the logarithm of film resistance versus reciprocal of temperature. These graphs showed two distinct regions such as low and high-temperature region. In the high-temperature region, the slope of the curve was more than the slope in the low-temperature region. The Arrhenius equation was used to calculate activation energies in high and low-temperature region. Activation energy is the energy sufficient for an electron in the valence band to jump in the conduction band. As seen from table II the values of activation energy at high temperature and at a low temperature of 0.1:0.1 MoO_3–In_2O_3 binary oxide film were 0.5774 eV and 0.1622 eV respectively. The activation energy at high temperature and at a low temperature for 0.1:0.2 MoO_3–In_2O_3 binary oxide films were 0.7976 eV and 0.1707 eV respectively. The 0.1:0.3 MoO_3–In_2O_3 binary oxide films had minimum activation energy (0.417 eV) in the high-temperature region among all tested binary oxide films. The low value of activation energy in the high-temperature region can be due to increased electron hopping.

The electrical properties certainly got modified due to the addition of MoO_3 in In_2O_3. The increase in MoO_3 dopant proportion increased the defects in base material In_2O_3. This caused a relative increase in resistivity. The surface oxygen vacancies might have worked as the charge carriers.

3.5. Gas sensing properties of In_2O_3:MoO_3 thin films

Figure 5 represents the variation of gas sensitivity of 0.1:0.1, 0.2:0.1, 0.3:0.1, 0.1:0.2, 0.2:0.2, 0.3:0.2, 0.1:0.3, 0.2:0.3, and 0.3:0.3 MoO_3–In_2O_3 binary oxide thin films for ethanol vapors, nitrogen dioxide (NO_2), carbon monoxide (CO), ammonia (NH_3) and liquefied petroleum gas (LPG). The temperature was varied in steps of 50°C and corresponding gas sensitivity was calculated using equation 5. Nearly all films showed maximum gas sensitivity at about 150°C. This was the optimum temperature for gas sensitivity. The optimum temperature is the temperature at which supplied thermal energy is just sufficient for an electron to jump from the valence band into the conduction band.

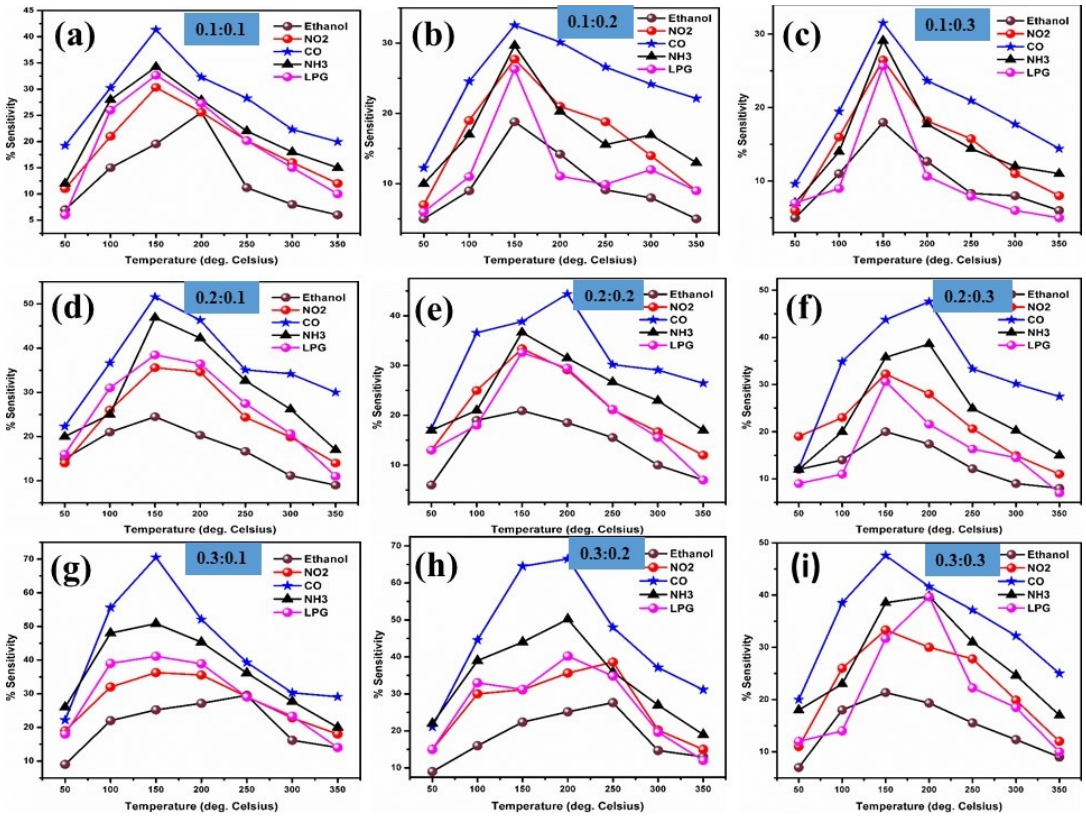

FIG. 5. Gas sensing response of (a) 0.1:0.1, (b) 0.1:0.2, (c) 0.1:0.3, (d) 0.2:0.1, (e) 0.2:0.2 (f) 0.2:0.3, (g) 0.3:0.1, (h) 0.3:0.2, and (i) 0.3:0.3 MoO_3–In_2O_3 binary oxide films

The 0.3N MoO_3 and 0.1N In_2O_3 binary oxide thin films showed 70.5 % response to the 300 ppm of CO gas at 150°C. This was maximum among the response of nine binary oxide combinations thin films. This sensitivity was

directly related to the minimum activation energy in high-temperature region exhibited by 0.3:0.1 MoO_3–In_2O_3 binary oxide films.

The gas response of 0.3:0.1 MoO_3:In_2O_3 binary oxide films with varying concentrations of CO was studied at 150°C. The sensitivity of the films for 50, 100, 150, 200, 250 and 300 ppm of CO was studied. Corresponding change in sensitivity versus time has been demonstrated in Fig. 6(a). It was obvious that with increase in ppm concentration of CO increased the gas sensitivity. As more target gas was available, more was the adsorption probability hence gas sensitivity increased. The films showed quick response (15s) and recovery (25s) time. This quick response may be due to increased adsorption due to increase in defects. Fast recovery was due to fast oxidation of the carbon monoxide.

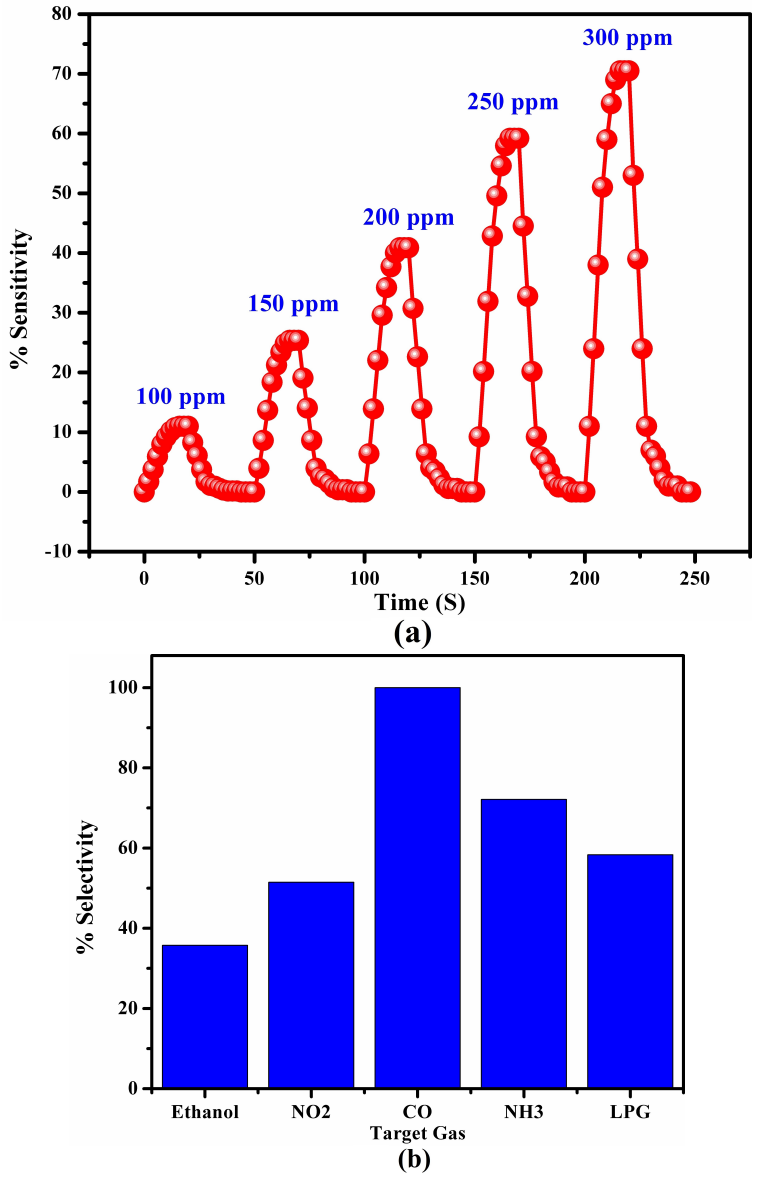

FIG. 6. (a) Sensitivity versus time for various ppm concentration of CO gas for 0.3:0.1 MoO_3–In_2O_3 binary oxide films at 150°C. (b) Percentage selectivity of 0.3:0.1 MoO_3–In_2O_3 binary oxide films for 300 ppm CO gas at 150°C

When films are exposed to multiple gases, the selectivity of the films to particular gas is the important factor. The selectivity for target gas was calculated using equation 6. The 0.3N MoO_3:0.1N In_2O_3 films showed excellent selectivity for CO against other tested gases as shown in Fig. 6(b).

3.6. CO sensing mechanism

Combustion processes in industries and cars generate toxic gases. CO is one of the main air pollutants. Once CO reacts with hemoprotein in human blood, the oxygen-carrying capability of the blood decreases. Excessive exposure to CO can even cause death. Thus CO sensing has its importance within the trendy industrial era [27].

Molybdenum oxide and indium oxide together improved CO gas sensitivity property. Numerous studies have projected multiple gas sensing mechanisms. Adsorption and desorption mechanism is one in many clarifications for gas sensing. Electron affinity is an important property of oxygen. Molecular oxygen (O^{2-}) or atomic form (O^{-}, O^{2-}) get adsorbed on MoO_3 surface. The adsorbed molecular oxygen at higher temperatures possesses low activation energy [28]. MoO_3 is a traditional n-type semiconductor. Comini et al. projected that once CO is introduced within the gas chamber, the exchange of electrons takes place between the semiconductor and ionosorbed oxygen species inflicting a modification in resistance [29].

Some reports projected that the lattice oxygen that competes for a significant role in gas sensing. Oxygen at lattice sites oxidized the target gas (CO) molecule catalytically. After CO desorption, the oxygen vacancies were created at the surface of the molybdenum and indium oxide. These oxygen vacancies at the surface were consummated by the oxygen within the inner region of the molybdenum oxide. This method caused changes in the conductivity of indium oxide [28].

4. Conclusion

In the current study, molybdenum oxide doped In_2O_3 (MoO_3:In_2O_3) binary oxide thin films have been synthesized successfully via a spray pyrolysis technique. The surface morphology, electrical and gas sensing properties of the MoO_3: In_2O_3 binary oxide thin films was investigated. The maximum resistivity of 17.50×10^3 Ωm was observed for the 0.3N MoO_3 and 0.1N In_2O_3 films with 0.3N MoO_3. The values of resistivity were found between 17.50×103^4 Ωm and 13.125×10^3 Ωm. The various concentration of Mo-doped In_2O_3 film for gas sensing properties has been studied in details. MoO_3–In_2O_3 film prepared with 0.3N MoO_3 as dopant showed a good response to 300 ppm of CO at operating temperature 150°C. It exhibited high selectivity to CO gas. The response and recovery time for CO gas were found 15s and 25s respectively. The grain size and particle size of the deposited film were decreased by adding MoO_3 in range 0.1N–0.3N.it has been analyzed by XRD and SEM. It has been observed that sensitivity for CO gas increased by increased in resistivity of film and a decrease in grain size and particle size.

Acknowledgment

Authors are thankful to Management of Arts, Science, Commerce College, Kalwan (Manur) Nashik, Principal, MSG College, Malegaon for providing research infrastructure and Department of Physics, Savitribai Phule Pune University, Pune for the characterization facility.

References

[1] Takada T., Suzuki K. and Nakane M. Highly sensitive ozone sensor, *Sensors & Actuators B: Chemical*, 1993, **13–14**, P. 404–407.

[2] Galdikas A., Marturas Z., Setkus A. SnInO-based chlorine gas sensor. *Sensors and Actuators B: Chemicl*, 1992, **7**, P. 633–636.

[3] Korotcenkov G., Cerneavschi A., Brinzari V., Cornet A., Morante J., Cabot A., Arbiol J. Ozone sensing properties of In2O3 films deposited by spray pyrolysis. *Moldavian Journal of Physical Sciences*, 2002, **1**(3), P. 24–27.

[4] Kiriakidsis G., Bender M., Katsarakis N., Gogaoudakis E., Hourdakis E., Douloufakis E., Cimalla V. Ozone sensing properties of polycrystalline indium oxide films at room temperature. *Physica Status Solidi (a)*, 2001, **185**(1), P. 27–32.

[5] Seffes H., Imawan C., Solzbacher F., Obermeir E. Enhancement of NO_2 sensing properties of In_2O_3-based thin films using Au or Ti surface modification. *Sensors and Actuators B: Chemical*, 2001, **78**(1-3), P. 106–112.

[6] Scharnagl K., Anothainart K., Fuchs A., Winter R., Zimmer M., Wlodarski W., Doll T., Eisele I. Room temperature ozone detection: comparison between indium oxide and potassium iodide. *Proceedings of the 13-th European Conference on Solid State Transducers Eurosensors XIII*, The Hague, The Netherlands pp. 255–258, 12–15 September 1999.

[7] Faglia G., Allieri B., Comini E., Depera L.E., Sangaletti L., Sberveglieri G. Electrical and structural properties of RGTO-In_2O_3 sensors for ozone detection. *Sensors Actuators B: Chemical*, 1999, **57**, P. 188–191.

[8] Gurlo A., Ivanovskaya M., Barsan N., Weimar U., Gopel W. In_2O_3 and In_2O_3–MoO_3 thin film semiconductor sensors: interaction with NO_2 and O_3. *Sensors & Actuators B: Chemical*, 1998, **47**, P. 92–99.

[9] Ivanovskaya M., Bogdanov P., Faglia G., Sberveglieri S. The features of thin films and ceramic sensors at the detection of CO and NO_2. *Sensors & Actuators B: Chemical*, 2000, **68**, P. 344–350.

[10] Lee H.J., Song J.H., Yoon Y.S., Kim T.S., Kim K.J. and Choi W.K. Enhancement of CO sensitivity of indium oxide-based semiconductor gas sensor through ultra-thin cobalt adsorption. *Sensors & Actuators B: Chemical*, 2001, **79**, P. 200–205.

[11] Yamaura H., Moriya K., Miura N. and Yamazoe N. Mechanism of sensitivity promotion in CO sensor using indium oxide and cobalt oxide. *Sensors & Actuators B: Chemical*, 2000, **65**, P. 39–41.

[12] Yamaura H., Jinkawa T., Tamaki J., Moriya K., Miura N., Yamazoe N. Indium oxide based gas sensor for selective detection of CO. *Sensors & Actuators B: Chemical*, 1997, **35–36**, P. 325–332.

[13] Ferroni M., Guidi V., Martinelli G., Nelli P., Sacerdoti M., Sberveglier G. Characterization of a molybdenum oxide sputtered thin film as gas sensor. *Thin solid films*, 1997, **307**, P. 148–151.
[14] Ferroni M., Guidi V., Martinelli G., Nelli P., Sacerdoti M., Sberveglier G. MoO_3 based sputtered thin films for fast NO_2 detection. *Sensors &. Actuators B: Chemical*, 1998, **48**, P. 285–288.
[15] Chung W.Y., Sakai G., Shimanoe K., Miura N., Lee D.D., Yamazoe N. Preparation of indium oxide thin film by spin-coating method and its gas-sensing properties. *Sensors &. Actuators B: Chemical* , 1998, **46**, P. 139–145.
[16] Liess M. Electric-field-induced migration of chemisorbed gas molecules on a sensitive filma new chemical sensor. *Thin Solid Films*, 2002, **410**, P. 183–187.
[17] Tamaki J., Naruo C., Yamamoto Y., Matsuoka M. Sensing properties to dilute chlorine gas of indium oxide based thin film sensors prepared by electron beam evaporation. *Sensors & Actuators. B: Chemical*, 2002, **83**, P. 190–194.
[18] Kiriakids G., Bender M., Katsarakis N., Gagaoudakis E., Hourdakis E., Douloufakis E., Cimalla V. Ozone sensing properties of polycrystalline indium oxide films at room Temperature. *Physica Status Solidi A*, 2001, **185**, P. 27–32.
[19] Liu X., Jiang L., Jiang X., Tian X., Huang Y., Hou P., Zhang S., Xu X. Design of superior ethanol gas sensor based on indium oxide/molybdenum disulfide nanocomposite via hydrothermal route. *Applied Surface Science*, 2018, **447**, P. 49–56.
[20] Li H., Ahn S.H., Park S., Cai L., Zhao J., He J., Zhou M., Park J., Zheng X. Molybdenum disulfide catalyzed tungsten oxide for on-chip acetone sensing. *Applied Physics Letters*, 2016, **109**(13), P. 133103.
[21] Zhang D., Chang H., Sun Y., Jiang C., Yao Y., Zhang Y. Fabrication of platinum-loaded cobalt oxide/molybdenum disulfide nanocomposite toward methane gas sensing at low temperature. *Sensors and Actuators B: Chemical*, 2017, **252**, P. 624–632.
[22] Ahire D.V., Shinde S.D., Patil G.E., Thakur K.K., Gaikwad V.B., Wagh V.G., Jain G.H. Preparation of MoO_3 thin films by spray pyrolysis and its gas sensing performance. *International Journal On Smart Sensing and Intelligent Systems*, 2012, **5**(3). P. 592–605.
[23] Deshmane V.V., Patil A.V. Structural and Electrical Properties of Synthesized Undoped Iron Oxide Films. *International Journal of Chemical & Physical Sciences, Special Issue 12 ICAFM (Part-II)*, 2018, **7**, P. 425–430.
[24] Deshmane V.V., Patil A.V. Study of In_2O_3 & α-Fe_2O_3 nano-composite as a petrol vapor sensor. *Material research express*, 2019, **6**(2), P. 025904.
[25] Deshmane V.V., Patil A.V. Synergy of semiconductor (Hematite) & catalytic (Ni) properties enhance gas sensing behavior to NO_2. *Material research express*, 2019, **6**, P. 072910.
[26] Mohammadi S., Abdizade H., Golobostanfard M.R. Structural, Optical and Electrical Characterization of Mo Doped In_2O_3 Thin Films Prepared via Sol-Gel Spin Coating Technique. *Advanced Materials Research*, 2012, **576**, P. 607–610.
[27] Hou L., Zhang C., Li L., Du C., Li X., Kang X.F., Chen W. CO gas sensors based on p-type CuO nanotubes and CuO nano-cubes: Morphology and surface structure effects on the sensing performance. *Talanta*, 2018, **188**, P. 41–49.
[28] Arachchige M., Zappa H.M.M., Poli D.N., Gunawardhana N., Comini E. Gold functionalized MoO_3 nano flakes for gas sensing applications. *Sensors and Actuators B: Chemical*, 2018, **269**, P. 331–339.
[29] Comini E., Yubao L., Brando Y., Sberveglieri G. Gas sensing properties of MoO_3 nanorods to CO and CH_3OH. *Chemical Physics Letters*, 2005, **407**(4-6), P. 368–371.